### Title
Influence of nanoparticle doping on the colloidal stability and toxicity of copper oxide nanoparticles in synthetic and natural waters




### Authors
Adeleye, Adeyemi S
Pokhrel, Suman
Mädler, Lutz
et al.



### Publication Date
2018-04-01

### DOI
10.1016/j.watres.2017.12.069

Peer reviewed

Water Research 132 (2018) 12–22

Contents lists available at ScienceDirect

Water Research

journal homepage: www.elsevier.com/locate/watres

# Influence of nanoparticle doping on the colloidal stability and toxicity of copper oxide nanoparticles in synthetic and natural waters

Adeyemi S. Adeleye [a, c, 1], Suman Pokhrel [b, c], Lutz Mädler [b, c], Arturo A. Keller [a, c, *]

[a] Bren School of Environmental Science & Management, University of California, California 93106–5131, United States
[b] Foundation Institute of Materials Science (IWT), Department of Production Engineering, University of Bremen, Bremen, Germany
[c] University of California Center for Environmental Implications of Nanotechnology, Santa Barbara, California United States

ARTICLE INFO

*Article history:*
Received 1 July 2017
Received in revised form
22 December 2017
Accepted 24 December 2017
Available online 28 December 2017

*Keywords:*
Copper oxide nanoparticle
Natural waters
Environmental fate
Toxicity
Transformation

ABSTRACT

Engineered nanoparticles (NPs) are often doped with other elements to improve their functionality and, at times, physical and/or chemical stability. However, the effect of doping on the environmental implications of NPs is not well-understood. We investigated the colloidal stability and effects of CuO NPs doped with Fe (0–10%). Colloidal stability of the Fe-doped CuO NPs in aqueous media, as determined by critical coagulation concentrations of NaCl, decreased with increased Fe-doping. However, decrease in the overall particle density led to slower sedimentation of Fe-doped CuO NPs than would have been predicted from their aggregation behavior. Fe-doping significantly affected CuO dissolution ($p < .001$), promoting Cu leaching out from the doped NPs due to increased reactivity at neutral pH and increased surface area with Fe-doping. Fe-doping did not increase the toxicity of CuO to a marine phytoplankton, *Isochrysis galbana*, despite promoting ionic Cu release. Total suspended Cu was dominated by dissolved Cu complexes in seawater and particulate Cu in freshwater. Based on the abundance of different size fractions analyzed in freshwater, the particles detected in water suspension were mostly (≥50%) larger than 200 nm in diameter. However, these large-sized particles are mainly composed of aggregated nanosized particles held together by van der Waals attraction.



## 1. Introduction

Several applications of engineered nanoparticles (NPs) require that they are combined with other materials, which may be mere matrices or co-primary ingredients. The use of these nanocomposites has been widely reported in the literature (Adeleye et al., 2016b; De Volder et al., 2013; Wagner, 2007; Wang et al., 2011a). In addition, the composition of NPs may be intentionally modified to form nanohybrids, doped NPs or composites in order to improve their functionality or reduce unwanted properties (Fairbairn et al., 2011; Wang et al., 2011a; Xia et al., 2011). For instance, one of the primary applications of copper NPs is in electronics and optics (Keller et al., 2013), and the incorporation of small amounts of Fe enhances the applications of CuO in magnetic storage devices (Keller et al., 2013; Yin et al., 2010). Doped NPs have wide applications in fields including medicine, biotechnology, energy, environmental science, etc.; and their uses include chemical sensing/biological imaging, catalysis, and environmental remediation (Adeleye et al., 2016a; Chen et al., 2004; Thakar et al., 2007; Wang et al., 2011a), However, doping may also influence the physicochemical properties of the NPs, and thus, their environmental implications (Fairbairn et al., 2011; Xia et al., 2011). For instance, the dissolution and toxicity of ZnO NPs were significantly reduced when they were doped with Fe (Fairbairn et al., 2011).

Recently, several studies focused on the environmental implications of copper-based NPs due to the toxicity of copper, and the increasing application of copper NPs in consumer products (Adeleye, 2015; Adeleye et al., 2016b; Ingle et al., 2014; Keller et al., 2017; Midander et al., 2009; Wang et al., 2013; Zhao et al., 2016b). Most of these studies, however, researched single elements (e.g. Cu NPs) or common compounds of copper (e.g. CuO NPs). While these studies provide knowledge useful for predicting the environmental hazard of the basic NPs, a good understanding of the fate and transformation of doped NPs, nanocomposites, and nanohybrids is necessary since nanomaterials are often used and will be

* Corresponding author. Bren School of Environmental Science & Management, University of California, California 93106–5131, United States.
*E-mail address:* keller@bren.ucsb.edu (A.A. Keller).
[1] Present Address. National Research Council Research Associate, Atlantic Ecology Division, US Environmental Protection Agency, Narragansett, Rhode Island, United States.

https://doi.org/10.1016/j.watres.2017.12.069
0043-1354/

introduced into the environment in these forms. Studies investigating the fate of doped NPs are currently rare.

In order to exhaustively investigate how the human health and environmental implications of NPs may be influenced by doping them, our research consortium synthesized CuO NPs doped with Fe (0–10%) using flame spray pyrolysis techniques. The fate and effects of the pure CuO and Fe-doped CuO NPs were then carefully studied in the two important systems—biological and environmental. In a recently published article summarizing the finding in biological media, Naatz and coworkers reported that Fe-doping of CuO reduced the release of toxic Cu ions in biological media (Naatz et al., 2017). This article reports our findings on the environmental implications of the same pure and Fe-doped CuO NPs. The aggregation, dissolution, and transformation of the NPs were thoroughly investigated in both simple aqueous media and natural waters. Furthermore, the NPs were exposed to an axenic marine phytoplankton culture in order to determine their potential toxicity to this important class of organisms.

## 2. Experimental section

### 2.1. Nanoparticle synthesis

The synthesis of pure and Fe-doped CuO NPs was carried out using in-house built flame spray pyrolysis (George et al., 2010; Kemmler et al., 2013; Pokhrel et al., 2010). Copper naphthenate (Strem Chemical, 99.9% pure) was used as a precursor, with or without iron napthenate (12% Fe by metal, Strem, 99.9% pure). All the precursors were diluted with xylene (Strem Chemicals, 99.95% pure) to obtain a total metal concentration of 0.5 M. To synthesize the library of CuO doped with 0, 2, 6, and 10% Fe (hereafter referred to as 0%Fe-CuO, 2%Fe-CuO, 6%Fe-CuO, and 10%Fe-CuO, respectively), a 50 mL portion of 0.5 M copper naphthenate was separately mixed with 1.15–5.7 mL of 0.5 M iron naphthenate. Each liquid precursor was delivered to the nozzle tip by a syringe pump at a flow rate of 5 mL/min by atomising the precursor solution with dispersant $O_2$ at a flow rate of 5 mL/min, and maintaining a pressure drop of 1.5 bar at the nozzle tip. Combustion of the dispersed droplets was initiated by the co-delivery of $CH_4$ and $O_2$ (1.5 L/min, 3.2 L/min) to sustain a flame. The particles were collected from the 257 mm glass filters placed at a distance of 60 cm from the nozzle. Commercially-available CuO NPs (denoted CuO-SA) were obtained from Sigma Aldrich to compare with the one synthesized in-house (i.e. 0%Fe-CuO). In addition, Cu and $Cu_2O$ NPs (denoted *n*Cu and *n*$Cu_2O$), respectively) were obtained from US Nanomaterials (Houston, TX) to understand how the fate of the synthesized library of pure and Fe-doped CuO NPs compare with these other copper-based NPs.

### 2.2. X-ray diffraction and Brunauer–Emmet–Teller surface area analyses

For the X-ray diffraction measurements, the NPs (0–10%Fe-doped CuO) were loaded into a Bruker D8 diffracting system. The diffractometer was configured in Bragg-Brentano geometry equipped with a primary Johansson monochromator producing Ni-filtered Cu-$K_\alpha$ ($\lambda = 0.154$ nm) radiation. A ~0.1° fixed divergence, 4° primary, 2.5° secondary soller slits, and LynxEye detector (position sensitive in a range of 3° 2$\theta$ with 192 channels, yielding a channel width of 0.01563° 2$\theta$) was used (Dreyer et al., 2016; Pokhrel et al., 2015). Continuous scans were applied with an integration step width of ~0.03° 2$\theta$ and 30 s per step. The determination of the average crystallite sizes ($d_{XRD}$) was achieved by the line-broadening analysis during the Rietveld refinement of the x-ray patterns. The instrumental contribution to the peak broadening was corrected using $LaB_6$ as an instrumental standard.

The adsorption-desorption isotherms of nitrogen Brunauer-Emmett-Teller (BET) were measured at 77 K using a Quantachrome NOVA 4000e and Autosorb-1 gas sorption system as a function of relative pressure $P/P_o$ over the range of 0.01–0.99. Prior to the measurement, the sample was outgassed at 200 °C under vacuum to determine the specific surface areas. The pore volume was estimated from the nitrogen uptake at $P/P_o = 0.99$. Data were obtained by exposing or removing a known quantity of adsorbing gas in or out of a sample cell containing the solid adsorbent maintained at constant liquid nitrogen temperature.

### 2.3. Transmission electron microscopy

The NPs (2–5 mg) were dispersed in absolute ethanol followed by ultrasonication for 1 h. A drop from the resulting dispersion was placed on a transmission electron microscopy (TEM) grid using an eye dropper and dried at room temperature. High resolution transmission electron microscopy images (HRTEM) were obtained using a FEI Titan 80/300 microscope equipped with a Cs corrector for the objective lens, high angle annular dark field detector (HAADF), GATAN post-column imaging filter and a cold field emission gun operated at an accelerating voltage of 300 kV.

### 2.4. Particle surface charge

The surface charge of the NPs was estimated by measuring their zeta ($\zeta$) potential using a Zetasizer ZS90 (Malvern, UK). For $\zeta$ potential measurements, stocks of the particles were prepared in deionized (DI) water (Barnstead Nanopure; 18.2 MΩ cm). Aliquots were taken from the stock to prepare samples (50 mg/L) in freshwater (pH 7.1). The freshwater was made in accordance with EPA method 1003.0 with 1 mg-C/L Suwannee River natural organic matter (SRNOM) (Adeleye and Keller, 2014; EPA, 2002). $\zeta$ potential was not measured in seawater due to the high ionic strength, which burns out zeta cells during measurements. Additional measurements were carried out in DI water at several ionic strength conditions (0, 10 and 50 mM NaCl) at pH 5.5 (2 mM acetate buffer) and pH 8.2 (2 mM carbonate buffer). The isoelectric point (IEP) of the particles in 1 mM NaCl was determined by adjusting pH with dilute HCl and NaOH (0.01–0.1 mM) and measuring $\zeta$ potential using the Zetasizer. Multiple samples were used for titrations to different pH values so as to minimized the amounts of titrants used, and thus, changes in ionic strength of the nanoparticle suspensions.

### 2.5. Aggregation kinetics

The critical coagulation concentrations (CCC) of NaCl were determined for the synthesized pure and Fe-doped CuO NPs as described previously (Adeleye et al., 2014; Adeleye and Keller, 2014), and summarized in Supplementary Information (SI) section A1. For the analyses, particle concentration was 50 mg/L while pH was held at either 5.5 (acetate buffer) or 8.2 (carbonate buffer), with or without SRNOM (1 mg-C/L). Aggregation was studied at 20 °C via time-resolved dynamic light scattering (DLS) using the Zetasizer. Data were collected in triplicates at 30 s intervals for 1 h or until the hydrodynamic diameter was double the initial value. For comparison, the CCC of NaCl was also determined for CuO-SA and *n*$Cu_2O$ in similar conditions as the pure and Fe-doped CuO NPs. The CCC of NaCl was not determined for *n*Cu due to the particle's high polydispersity and poor stability in aqueous media (Adeleye et al., 2014; Conway et al., 2015).

### 2.6. Dissolution, sedimentation, and transformations

The dissolution of all the NPs was studied in conditions simulating the surface of natural waters (14:10 light:dark, ~6000 Lux, 140 rpm) (Bennett et al., 2013). Temperature was held constant at 20 °C throughout the study, which was carried out at two initial particle concentrations—low (500 μg/L) and high (5 mg/L). Initial volume was 300 mL, and all experimental conditions were tested in triplicates. Aliquots for sampling were removed from the top 1 cm of the aqueous phase; thus only dissolved ions and suspended particles were collected for analyses. To reduce the possibility of contamination from metal leaching, glassware was avoided in this study and all pipette tips were acid-leached prior to use. Containers were either certified metal-free (VWR International, Radnor, PA) or acid-leached before use.

#### 2.6.1. Low concentrations studies

These experiments were carried out to estimate the fate of the NPs at concentrations similar to what is expected in the natural waters (low ppb). Dissolved, 100 nm, and 200 nm Cu fractions present in the aqueous phase were estimated similar to the method used in a previous study (Adeleye et al., 2016b). In brief, dissolved fractions were separated from the particulate fractions with Millipore Amicon Ultra-4 3 kDa centrifugal filter tubes, which retains particles greater than 1.5 nm. The 100 nm fraction (diameter ≈ 1–100 nm) was defined as the fraction that passed through a 0.1 μm filter (Whatman, UK), accounting for the dissolved fraction. 200 nm fractions (diameter ≈ 100–200 nm) were determined by subtracting the dissolved and 100 nm fractions from the fraction obtained by filtering with 0.2 μm filters (Thermo Scientific, Waltham, MA). Particles greater than 200 nm were defined as bulk. In addition, aliquots were measured without filtration to determine total suspended Cu (dissolved + particulate). Cu was quantified via inductively coupled plasma-mass spectrometry (ICP-MS) using an Agilent 7900 ICP-MS (Santa Clara, CA). The detection limit ranged from 0.005 μg/L in clean water to 0.96 μg/L in high salt matrix. Dissolved Fe was not measured as preliminary studies conducted in freshwater and seawater showed no significant leaching of Fe from the Fe-doped CuO NPs at the concentrations tested. Single-particle ICP-MS (spICP-MS) was also used to confirm the presence of nanosized Cu fractions throughout the study using the Agilent 7900 ICP-MS (Adeleye et al., 2016b). sp-ICP-MS analyses were performed in time resolved analysis (TRA) mode using an integration time of 0.1 ms per point with no settling time between measurements. NIST 8012 Au reference material (nominal diameter = 30 nm) was employed for determination of plasma's nebulization efficiency. A NIST-traceable Cu standard (concentration = 1 μg/L) was used to determine the elemental response factor. Method setup and data analyses were carried out in the Single Nanoparticle Application Module ICP-MS MassHunter software (Agilent Technologies, Santa Clara, CA). This study was conducted for 14 d in both EPA freshwater and seawater. Seawater was collected from the Pacific Ocean (at Santa Barbara, CA) and filtered (0.2 μm) before use. Only 0%Fe-CuO and 10%Fe-CuO were used for this study. Background Cu in freshwater and seawater was not detectable.

#### 2.6.2. High concentration studies

This study was carried out at the ppm range (5 mg/L) to allow for more precise detection of the different fractions (dissolved, 100 nm, and 200 nm) of Cu (from the NPs) via filtration techniques coupled with ICP-MS as explained earlier. This study was conducted for 30 d using the four synthesized pure and Fe-doped CuO NPs (0, 2, 6, and 10% Fe), and the three commercial NPs in EPA freshwater. Particles in the aliquots collected from the supernatants of samples on Days 0 and 30 were visualized using a FEI Tecnai G2 Sphera 200 kV TEM equipped with an Oxford INCA x-sight probe for energy-dispersive X-ray spectroscopy (EDS).

### 2.7. Toxicity to marine phytoplankton

The influence of Fe-doping on the potential ecological effects of CuO NPs was investigated by studying the toxicity of 0%Fe-CuO and 10%Fe-CuO to *Isochrysis galbana*. Phytoplankton are primary producers in aquatic systems, and are typically used to evaluate the environmental impacts of chemicals (including those that are copper-based) in both freshwater and marine systems. Axenic cultures were obtained from the National Center for Marine Algae and Microbiota (Bigelow Laboratory for Ocean Sciences, East Boothbay Harbor, ME), and were maintained in standard media (f/2) made with 0.2 μm-filtered natural seawater as described previously (Adeleye et al., 2016b). Inoculants were cultured for 5–7 d and initial cell density was kept at 2–3x$10^4$ cells/mL. All experiments were conducted at 20 °C, 34 ppt salinity, under cool white fluorescent lights (14 : 10 light : dark, ~6000 Lux) for 5 d. Cell densities were measured every 24 h using a Trilogy fluorometer (Turner Designs, Sunnyvale, CA), using *in vivo* chlorophyll fluorescence as a surrogate. *In vivo* chlorophyll fluorescence was converted to cell numbers using a calibration curve based on cell counts done with a hemacytometer (Reichert, Buffalo NY). Experiments were run in 125 mL polycarbonate flasks, media volume 80 mL, and were mixed at 120 rpm on a rotary shaker (New Brunswick Scientific, NJ) to allow for gas exchange through the filter-covered vents in flask caps. Additional experiments were conducted using CuO-SA in order to compare its effects with that of 0%Fe-CuO. Each particle was tested in triplicate at 0, 0.05, 0.1, 1, 5, and 10 mg/L exposure concentration. Adverse effects of the NPs were assessed via growth inhibition and reactive oxygen species (ROS) production.

#### 2.7.1. Growth inhibition

The average specific growth rate of the algae for the duration of exposure was calculated according to the following logistic equation:

$$\mu_{i-j} = \frac{\ln X_i - \ln X_j}{t_i - t_j}\left(day^{-1}\right) \quad (1)$$

where $\mu_{i-j}$ is the average specific growth rate from time $i$ to $j$; $X_i$ and $X_j$ are the cell densities at time $i$ and $j$, respectively; and $t_i$ and $t_j$ are the initial time of exposure and final time of exposure, respectively. Percentage inhibition of growth was calculated as:

$$I = \frac{\mu_C - \mu_T}{\mu_C} \times 100 \quad (2)$$

where $I$ is the percent inhibition in average specific growth rate; $\mu_C$ is the average specific growth rate in the control group, and $\mu_T$ is the average specific growth rate for the treatment.

#### 2.7.2. Cellular reactive oxygen species (ROS)

To investigate whether the cells of *I. galbana* were in oxidative stress upon their exposure to the NPs, total ROS level was quantified after 5 d. Total ROS produced in the organisms was assessed by incubating the cells in black 96-well plates containing carboxy-2′,7′-dichloro-dihydro-fluorescein diacetate ($H_2$DCFDA) probe (Invitrogen Molecular Probe, Eugene, OR) in the dark for 45 min at 20 °C. $H_2$DCFDA can diffuse freely across cells membranes, and is popularly used as an indicator for ROS. ROS in the cells promote the oxidation of $H_2$DCFDA to yield the fluorescent product 2′,7′-dichlorofluorescein (DCF) (Hong et al., 2009; Ivask et al., 2015). The intensity of DCF fluorescence in the cells was measured at 485 nm

(excitation) and 530 nm (emission) using a Synergy H1 microplate reader (BioTek Instruments, Winooski, VT). The assay was performed for each of the triplicates cultures with each culture measured a minimum of four times. NP-only controls were also measured. ROS levels were evaluated according to equation (3) (Hong et al., 2009):

$$RR = \frac{F_T}{F_C} \times 100 \quad (3)$$

Where RR is relative ROS level (%), $F_T$ is the mean DCF fluorescence of NP-treated cells, and $F_C$ is the mean DCF fluorescence of control cells.

## 3. Results and discussions

### 3.1. Nanoparticles synthesis and characterization

The specific surface areas and BET primary particle sizes ($d_{BET}$) of pure and Fe-doped CuO NPs ranged from 81 (±1.8) to 90 (±4.5) $m^2/g$ and 10–12 nm, respectively (Fig. 1, Table 1). Fe-doping did not have much influence on primary particle size and morphology. The crystallite sizes extracted from Rietveld refinement of the XRD patterns were in the range of 9–12 nm, reasonably agreeing with the BET primary particle diameters (Table 1). The low resolution TEM micrographs of pure and Fe doped CuO NPs showed spherical particles. The crystal structure of the NPs was studied by probing a single particle via HRTEM imaging. The images showed single crystalline particles of 0–10%Fe-CuO NPs with well-developed lattice fringes. The lattice plane distances of 0.2529 (±0.003), 0.2514 (±0.003), 0.2528 (±0.003), 0.2498 (±0.003) nm were observed for 0, 2, 6, and 10% Fe-doped CuO NPs, respectively (Fig. 1).

The XRD patterns show sharp and well resolved reflections, indicating a monoclinic system (ICSD 69757) with $a = 0.46927$ nm, $b = 3.4283$ nm, $c = 5.1370$ nm, $\alpha = \gamma = 90°$, and $\beta = 99.546°$ (Naatz et al., 2017; Torres-Duarte et al., 2016). Increasing Fe-loading resulted in an increasing peak shift, indicating Fe-incorporation into the CuO lattice (Fig. 2). A peak shift of 0.35° was observed for 10% Fe-doped CuO across the entire $2\theta$ angles. The ionic radii of $Cu^{2+}$ is 0.71 Å in square planar geometry and it is not possible for $Fe^{2+}$, with a much larger ionic radius (0.77 Å), to substitute $Cu^{2+}$. $Fe^{3+}$ with a smaller ionic radius (0.63 Å) can easily substitute $Cu^{2+}$ in the lattice. Hence the oxidation state of Fe in the doped CuO NPs is most likely +3. Raman spectroscopy and electron loss spectroscopy (EELS) analyses confirmed the formation of $CuFe_2O_4$ in the Fe-doped of CuO NPs (Naatz et al., 2017). The isoelectric point of $CuFe_2O_4$ was reported as pH 4.1 in a previous study (Li et al., 2015). The amount of Fe present in each of the Fe-CuO NPs was confirmed via ICP-MS and energy-dispersive X-ray spectroscopy (Table A1). Elemental mapping via energy-filtered transmission electron microscopy (EFTEM) showed that Fe and Cu appeared to be homogeneously distributed throughout the Fe-CuO NPs at all Fe loadings (Naatz et al., 2017). The primary particle size of CuO-SA, *n*Cu and *n*Cu2O was 50 nm, 40 nm, and 18 nm, respectively. The full characterization of CuO-SA, *n*Cu and *n*Cu2O is presented in Table A2.

### 3.2. Surface charge measurements

At pH 5.5 the ζ potential of the 0–10% Fe-CuO NPs decreased in magnitude (became less positive) as Fe-doping increased. For instance, the ζ potential in 10 mM NaCl decreased from 24.1 ± 0.8 mV (represents mean ± standard deviation throughout the manuscript unless otherwise stated) for 2%Fe-CuO to 12.9 ± 0.6 mV for 10%Fe-CuO (Fig. 3 and Fig. A1). The addition of 1 mg-C/L of SRNOM reversed the ζ potential of the NPs from

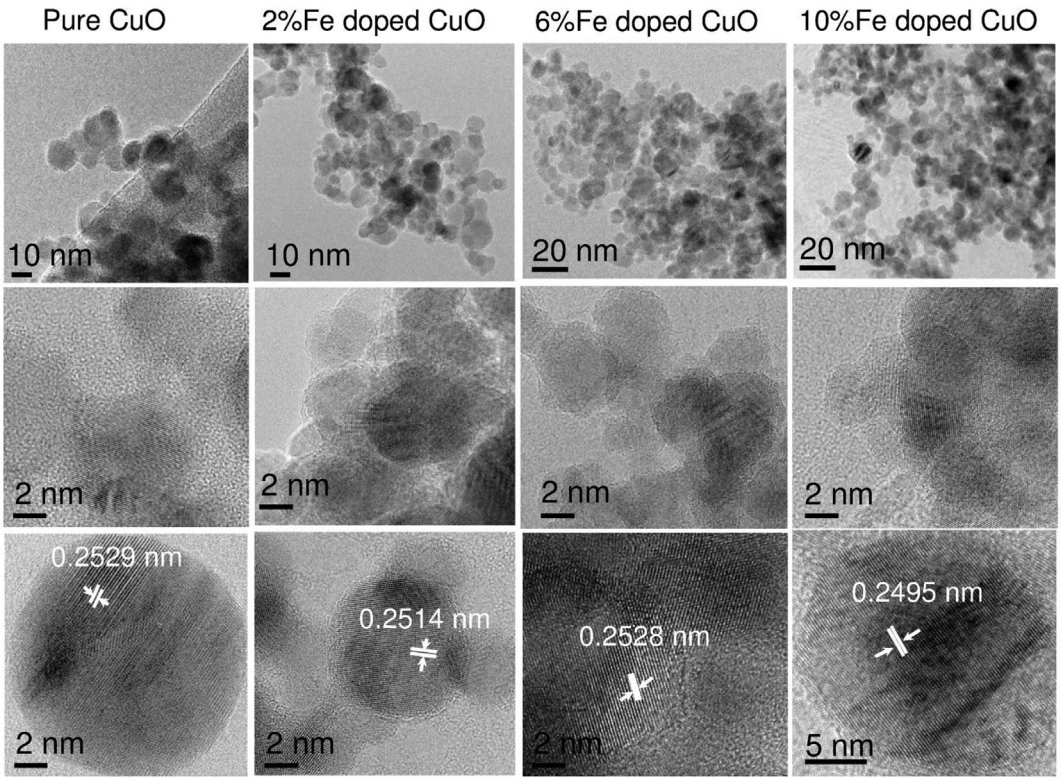


**Fig. 1.** TEM investigation of 0, 2, 6, and 10%Fe-CuO nanoparticles. Particles overview: HRTEM and the single particle morphology of 0%Fe-CuO (first row), 2% Fe-doped CuO (second row), 6% Fe-doped CuO (third row), and 10% Fe-doped CuO (fourth row).

**Table 1**
Primary Particle and crystallite size of pure and Fe-doped CuO nanoparticles.

| Characteristic | 0%Fe-CuO | 2%Fe-CuO | 6%Fe-CuO | 10%Fe-CuO |
|---|---|---|---|---|
| Crystallite size, $d_{XRD}$ (nm) | 8.9 (±1) | 9.2(±1) | 11.6(±1) | 11.4(±1) |
| Particle size, $d_{BET}$ (nm) | 11.8(±2) | 12.3(±2) | 10.3(±2) | 10.7(±2) |
| Hydrodynamic size (nm)[a] | 162.9 ± 3.5 | 145.1 ± 6.5 | 165.2 ± 11.9 | 157.7 ± 11.4 |
| Zeta potential (mV) [a, b] | −33.4 ± 0.9 | −32.5 ± 0.6 | −31.8 ± 1.0 | −30.6 ± 0.3 |
| Isoelectric point | ~ pH 9.8 | ~ pH 9.5 | ~ pH 9.2 | ~ pH 9.0 |
| Specific surface area ($m^2$/g) | 80.9(±5) | 77.6(±5) | 92.9(±5) | 90.4(±5) |

[a] Analyses were carried out in the presence of 2 mM carbonate buffer, pH 8.2.
[b] Measurements were carried out in the presence of 0.1 mM NaCl.

positive to negative at pH 5.5, suggesting a strong attractive interaction between the NPs and organic matter. In the presence of SRNOM, the ζ potential of the Fe-CuO NPs also decreased in magnitude with increased Fe-doping. But unlike in the absence of SRNOM when ζ potential became less positive, ζ potential was more positive with increased doping in the presence of SRNOM. This behavior suggests the ζ potential of the doped NPs shifted towards that of the dopant ($CuFe_2O_4$, ζ potential at pH 5.5 = -5.2 mV) as the amount of the dopant increased, with or without SRNOM present (Fig. 3). The Fe-CuO NPs were negatively charged in EPA freshwater (pH 7.1) with 1 mg-C/L SRNOM (Fig. A2). Similar to our observation in simple aqueous media, the ζ potential shifted towards that of $CuFe_2O_4$ (ζ potential = -8.5 mV at pH 7) as Fe-doping increased—decreasing in magnitude from -24.1 mV in 0% Fe-CuO to -14.3 mV in 10%Fe-CuO.

Dissolution of CuO NP should occur at pH 5.5, leading to the release of $Cu^{2+}$. The adsorption of these positively charged ions onto the surface of the NPs could play a role in the measured ζ potential, but the influence of the dissolved Cu ions is probably small due to the short ζ potential measurement time (3 min). The dopant in Fe-doped CuO, $CuFe_2O_4$, could be chemically unstable at acidic/near-neutral pH conditions, forming $CuFeO_2$ and $Fe_2O_3$ and dissolved metals (Ding et al., 2013; Kuan et al., 2015) as shown in equations (4) and (5):

$$CuFe_2O_4(s) \leftrightarrow Fe^{3+}(aq) + CuFeO_2(s) + 4H_2O(aq) + 3e^-(aq) \quad (4)$$

$$CuFe_2O_4(s) + 2H^+ \leftrightarrow Cu^{2+}(aq) + Fe_2O_3(s) + H_2O(aq) \quad (5)$$

$CuFeO_2$ and $Fe_2O_3$ could subsequently dissolve to form more Cu and Fe ions, as shown in equations (6)–(8):

$$CuFeO_2(s) + 4H^+(aq) \leftrightarrow Cu^+(aq) + Fe^{3+}(aq) + 2H_2O(aq) \quad (6)$$

$$Fe_2O_3(s) \leftrightarrow 2Fe^{2+}(aq) + 4e^-(aq) + 1.5O_2(aq) \quad (7)$$

$$Fe_2O_3(s) + 6H^+(aq) \leftrightarrow 2Fe^{3+}(aq) + 3H_2O(aq) \quad (8)$$

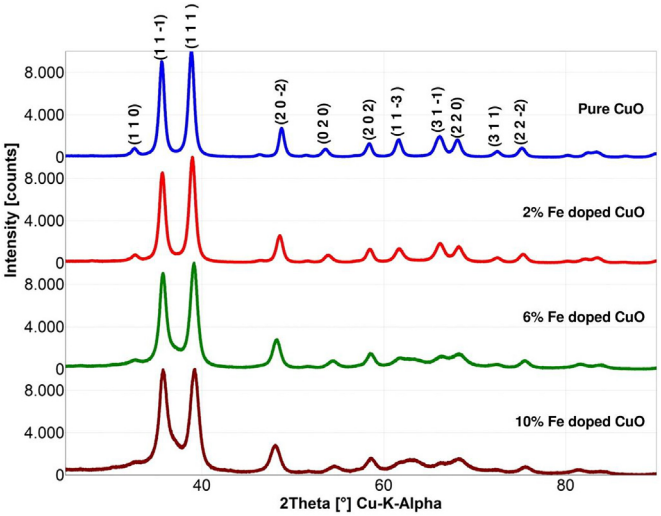


**Fig. 2.** X-ray diffraction patterns of pure and Fe-doped CuO nanoparticles.

Like in pure CuO NPs, both the Cu and Fe ions produced by these reactions can impart more positivity on surface of the Fe-doped particles if the ions adsorbed onto the surface of the particles. As shown in Fig. 3, however, the ζ potential of the Fe-doped NPs became less positive with increased Fe-doping. This suggests that the change in ζ potential due to Fe-doping was not driven by release of Cu and Fe ions but by the presence of $CuFe_2O_4$ in the particles. This is, again, probably due to the short timescale of ζ potential measurements.

The NPs were negatively charged at pH 8.2, which is still below their observed IEP (Table 1). The negative charge is likely due to the adsorption of hydroxyl ion or carbonate ions from the buffer onto the surface of the particles. Naatz et al. also reported negative charges on the surface of the Fe-doped CuO NPs in biological media (~pH 7.7) due to adsorption of serum albumin present in the media (Naatz et al., 2017). We observed a minimal shift in the ζ potential of the Fe-CuO NPs towards the ζ potential of $CuFe_2O_4$ at pH 8.2 (-12 mV) with increased Fe doping. At 50 mM NaCl for instance ζ potential decreased in magnitude from -23.3 ± 1.8 mV in 0%Fe-CuO to -19.0 ± 0.5 mV as Fe content increased to 10%. The impact of 1 mg-C/L SRNOM on the ζ potential of the Fe-CuO NPs at pH 8.2 was minimal as shown in Fig. 3, which is quite different than the behavior at pH 5.5. This is probably due to similarities in the surface charges of the NPs and the organic materials at pH 8.2, which leads to weaker attraction than at pH 5.5 where they have opposite charges. Regardless, the ζ potential of the NPs in the presence of SRNOM at pH 8.2 also shifted towards that of $CuFe_2O_4$ with increased Fe-doping.

CuO-SA (the commercial CuO NPs obtained from Sigma Aldrich) was also positively charged at pH 5.5 (14.2 ± 1.9 mV in 10 mM NaCl) and its charge was also inverted by 1 mg-C/L SRNOM (-34.7 ± 1.6 mV in 10 mM NaCl). At pH 8.2, CuO-SA was also negatively charged but much more so than all the Fe-CuO NPs. *n*$Cu_2O$ and *n*Cu were negatively charged at pH 5.5 and 8.2, with or without SRNOM (summarized in Fig. A1). In general, the ζ potential of the Fe-CuO NPs approached the ζ potential of the dopant ($CuFe_2O_4$) with increased doping in both simple aqueous media and natural water, although pH, ionic strength, and SRNOM also played important roles in determining the surface charge of the doped NPs. We hypothesized that this impact of doping on the surface charge of doped-CuO NPs will be observed in other doped NPs, especially if there is a clear difference in the surface charge of the NPs and the dopant.

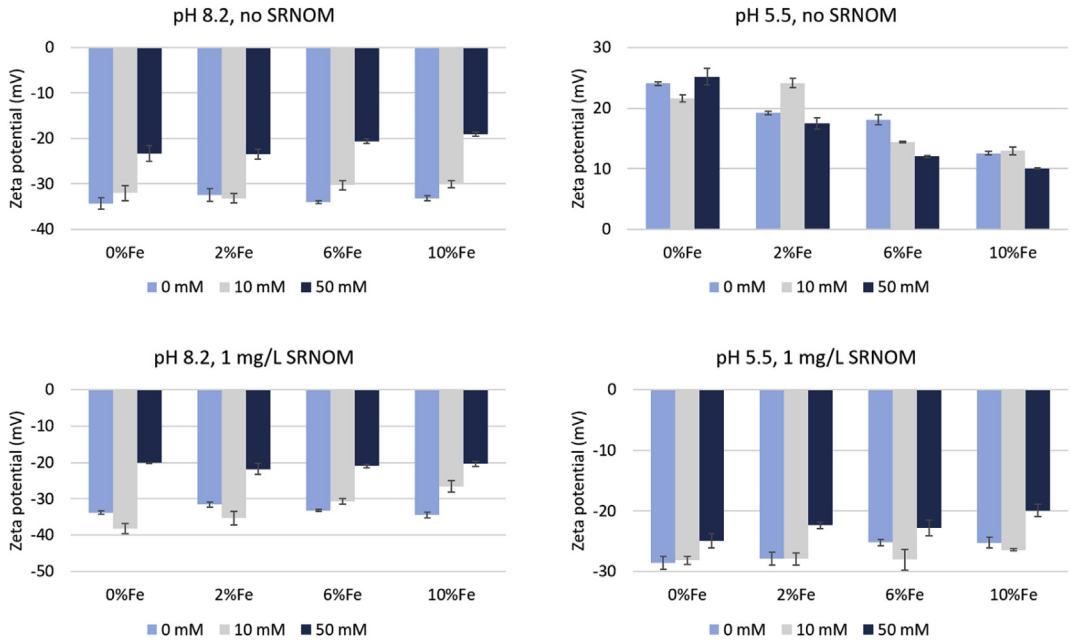


**Fig. 3.** Zeta potential of pure and Fe-doped CuO nanoparticles in the presence of NaCl (0, 10 and 50 mM NaCl) and SRNOM (1 mg-C/L) at pH 5.5 and pH 8.2.

### 3.3. Aggregation kinetics

To determine how Fe-doping affects the colloidal stability of the CuO NPs in aqueous media, the critical coagulation concentrations (CCC) of NaCl for the particles were determined at pH 5.5 and 8.2 with or without 1 mg-C/L SRNOM (summarized in Fig. 4). In general, the colloidal stability of the Fe-CuO NPs decreased with increased Fe-doping at both pH conditions, regardless of the presence of SRNOM. This agrees quite well with the trend observed in the ζ potential of the particles (which decreased in magnitude as Fe content increased). In the absence of NOM, the Fe-CuO NPs were more stable at pH 8.2 (where they were negatively charged) than at

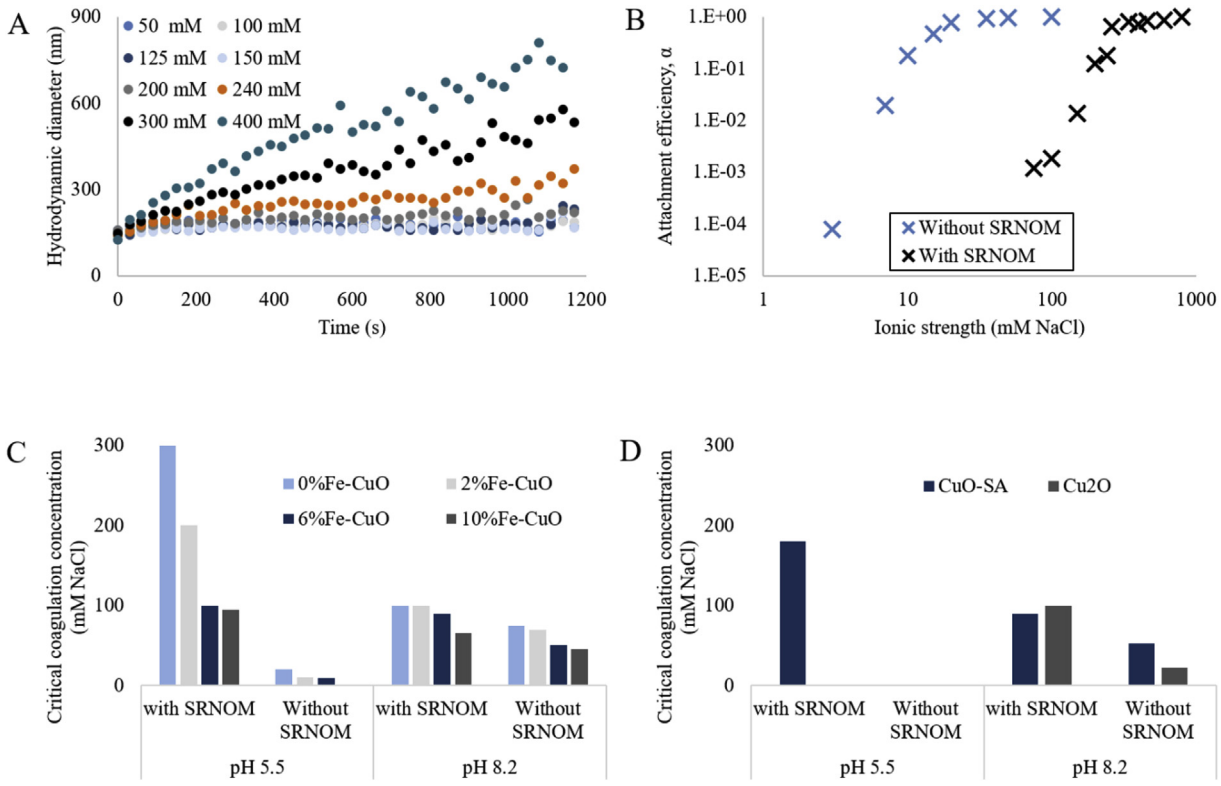


**Fig. 4.** (A) Typical aggregation kinetics data used to predict colloidal stability. Data was obtained using 0%Fe-CuO at pH 5.5 in the presence of 1 mg-C/L SRNOM. Legend represents NaCl concentrations in mM. (B) Comparison of critical coagulation concentrations (CCC, mM NaCl) with and without 1 mg-C/L SRNOM at pH 5.5. (C) Summary of the CCC of NaCl for (0–10%) Fe-doped CuO particles at pH 5.5 and 8.2 with and without 1 mg-C/L SRNOM. (D) CCC of NaCl for CuO-SA and $nCu_2O$. RSD for repeated experiments was <10%.

pH 5.5 (where they were positively charged). For instance, the CCC of 2%Fe-CuO was 10 mM NaCl at pH 5.5 and 70 mM NaCl at pH 8.2. Although the surfaces charges were opposite at the two pH values (Fig. 3), the difference in colloidal stability is due to differences in the magnitude of the charges. The ζ potential of the NPs exceeded -30 mV at most pH 8.2 conditions except in 50 mM NaCl (The typical threshold of colloidal stability is ±30 mV (Everett, 1988).). In addition, the reactivity of CuO and Fe-doped CuO in acidic conditions (equations (4)–(8)), which leads to the production of dissolved and particulate Cu and Fe species, may have contributed to the poor stability observed at pH 5.5. The presence of 1 mg-C/L SRNOM only led to slight increase in the CCC at pH 8.2 probably due to the aforementioned weaker attractive interactions. At pH 5.5 however, the CCC increased by an order of magnitude in the presence of the same amount of SRNOM (Fig. 4c). In addition to imparting electrostatic stability, NOM coating can also interfere with the reactivity of the particles, making them more stable at pH 5.5.

As shown here, similar to pristine CuO, Fe-doped CuO NPs followed the classic Derjaguin-Landau-Verwey-Overbeek (DLVO) theory of colloidal stability in the presence of NaCl. As ionic strength increased, the electrostatic energy barrier was reduced and the attachment efficiency of the Fe-doped NPs increased. The role of Fe-doping on the colloidal stability of Fe-CuO NPs was mainly a direct consequence of the effect of doping on the surface charge of the doped NPs. Thus, like most pristine NPs, the colloidal stability of doped NPs may be predictable from the effect of the dopant on the surface charge of the doped NPs.

CuO-SA was much less stable than 0%Fe-CuO at all conditions tested (Fig. 4c and d). In fact, CuO-SA was completely unstable without SRNOM at pH 5.5. While the CCC of NaCl for CuO-SA at pH 5.5 was determined as 180 mM NaCl when 1 mg-C/L SRNOM was present, the presence of SRNOM did not stabilize $n$Cu$_2$O at pH 5.5 (Fig. 4d). Instability of $n$Cu$_2$O (and $n$Cu) at pH 5.5 may be due to rapid dissolution of the NPs at this pH condition. The stability of CuO-SA and Cu$_2$O improved at pH 8.2; and similar to the Fe-CuO NPs, 1 mg-C/L SRNOM only slightly improved their stability at this pH condition.

### 3.4. Dissolution, sedimentation, and transformations

CuO NPs are not very soluble in natural waters (Adeleye, 2015; Adeleye et al., 2014; Conway et al., 2015; Keller et al., 2017), and this study was conducted to determine the influence of Fe-doping (present as $CuFe_2O_4$) on the dissolution of CuO NPs. Although both dissolved Cu and Fe species are typically produced during the reactions of $CuFe_2O_4$ in aqueous media at acidic and near neutral pH conditions (equations (4)–(8)), dissolved Fe was not detected in our experiments as stated earlier. This is probably due to the low amount of Fe in the doped NPs (10% or less), and more importantly, the dissolution of Fe is more suppressed than the dissolution of Cu from $CuFe_2O_4$ (Ding et al., 2013; Kuan et al., 2015).

This dissolution study was carried out at both relatively low (500 μg/L) and relatively high (5 mg/L) NP concentrations. The low concentration study was conducted in both freshwater (pH 7.1) and seawater (pH 8.1). Although a higher dissolution was expected in the freshwater, which had a lower pH (Equation (5) (Adeleye et al., 2014; Kuan et al., 2015),), the dissolved Cu detected in seawater after 14 d was almost double what was found in freshwater. This underscores the importance of complexation (with aqueous anions) in CuO/Fe-doped CuO dissolution. The full result and discussions for the low concentration experiment was provided in section A2 and Fig. A3-A5 in appendix. In addition, the low concentration study suggested that Fe-doping improved the dissolution of Fe-CuO

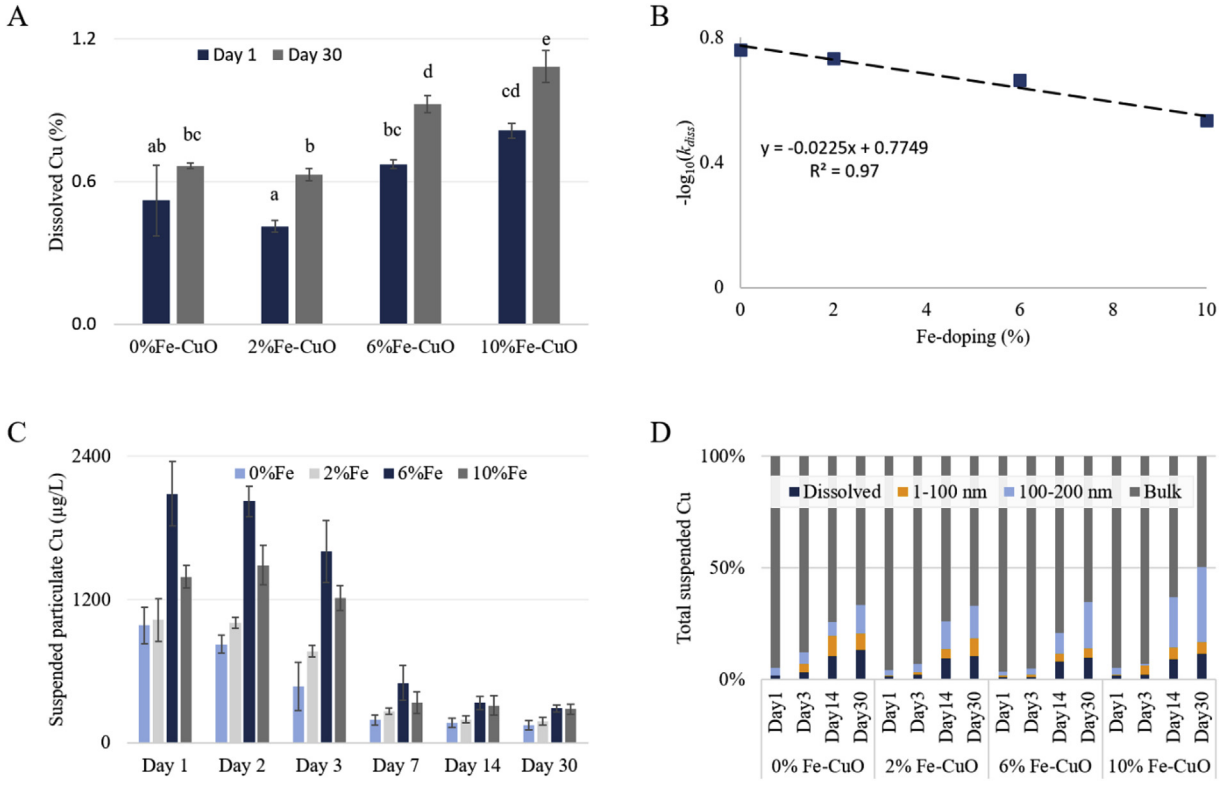


**Fig. 5.** (A) Dissolved Cu (%), determined as dissolved Cu concentration normalized by initial Cu content, on Days 1 and 30 from the 0–10% Fe-CuO nanoparticles. Letters represent statistical grouping based on Tukey's test; (B) Relationship between $-\log_{10}(k_{diss})$ and Fe-doping of CuO, where $k_{diss}$ is the dissolution rate determined after 96 h; (C) Suspended particulate Cu detected over 30 d; and (D) Fractions of Cu found in the aqueous phase over 30 d. For all experiments, initial particle concentration = 5 mg/L, and media = freshwater.

NPs. To confirm this initial observation, additional studies were carried out by exposing all the NPs into the EPA freshwater at particle concentrations of 5 mg/L to allow for clear observation of trends.

In general, we found that dissolved Cu was significantly dependent on Fe-doping ($p < .001$). Fig. 5a shows that increased Fe-doping led to higher solubility of Fe-CuO NPs in water. Although there was no significant difference between the dissolved Cu concentration detected in 0%Fe-CuO and 2%Fe-CuO after 24 h ($p = .77$), 6%Fe-CuO had a higher dissolved Cu concentration than 0%Fe-CuO and 2%Fe-CuO (though not statistically significant with $p = .56$ and .09, respectively). Dissolution of 10%Fe-CuO was significantly higher than both 0%Fe-CuO and 2%Fe-CuO ($p = .02$ for both), as well as 6%Fe-CuO (but not significantly, with $p = .64$). Average dissolved Cu concentration (in μg/L) measured 24 h after exposing the NPs to freshwater was $19.7 \pm 5.6$; $15.4 \pm 0.9$; $24.0 \pm 0.6$; and $27.9 \pm 1.1$ for 0%Fe-CuO, 2%Fe-CuO, 6%Fe-CuO, and 10%Fe-CuO, respectively. We observed similar trends up to 30 d, with average dissolved Cu concentration (in μg/L) of $25.2 \pm 0.5$; $23.5 \pm 1.0$; $33.1 \pm 1.3$; and $39.8 \pm 2.3$ for 0%Fe-CuO, 2%Fe-CuO, 6%Fe-CuO, and 10%Fe-CuO, respectively. As shown in Fig. 5b, there was a linear relationship between the % doping and $-\log_{10}(k_{diss})$, where $k_{diss}$ was defined as the dissolution rate after 96 h.

Naatz and coworkers recently reported very high dissolution (up to 70% within 24 h) of Fe-doped CuO in cell media (Naatz et al., 2017). In addition, they found decreased dissolution of CuO with increased Fe-doping in cell media. The dissolution of the Fe-doped CuO in the cell media were thought to be promoted by a decrease in media pH that resulted from interactions between the NPs and carbonate species present in media. In contrast, they also found dissolved mass ranging from $0.08 \pm 0.01\%$ (for 0%Fe-CuO) to $1.03 \pm 0.46\%$ (for 10%Fe-CuO) over 24 h when the NPs were exposed to DI water. Their observation in DI water agrees with this study, conducted in environmental media, in which we found (1) low dissolution of pure and Fe-doped CuO NPs: dissolved mass ranging from $0.52 \pm 0.15\%$ (for 0%Fe-CuO) to $0.81 \pm 0.03\%$ (for 10%Fe-CuO) in freshwater after 24 h; and (2) increased dissolution of Fe-doped CuO with increased Fe-doping. The differences between the dissolution kinetics of the Fe-CuO NPs in environmental and biological media emphasize the need to characterize nanomaterials and their composites in the media of interest to properly predict their fate and effects.

$CuFe_2O_4$ is somewhat unstable around pH 7 (Kuan et al., 2015), which can promote leaching of ions, especially Cu, from the doped CuO NPs (equations (4)–(6)). The promotion of Cu ion release is enhanced with increase in the % Fe-doping of CuO (content of $CuFe2O_4$). We hypothesize that the redox activity of the Fe-doped CuO NPs, coupled with increased specific surface area of the Fe-CuO NPs with increased Fe-doping (Table 1) led to increased solubility of the Fe-CuO NPs in environmental media.

The in-house prepared CuO (0%Fe-CuO) was more soluble (dissolved Cu after 24 h = $19.7 \pm 5.6$ μg/L) in freshwater than the commercial CuO obtained from Sigma Aldrich, CuO-SA (dissolved Cu after 24 h = $11.1 \pm 1.0$ μg/L) as shown in Fig. A6. Faster dissolution of 0%Fe-CuO is mainly due to its smaller size (12 nm compared to ~50 nm for CuO-SA) and thus larger surface area (80.9 $m^2$/g compared to 12.3 $m^2$/g for CuO-SA). In general, the (statistically significant) trend of dissolution for the 7 NPs tested in this study—based on dissolved Cu detected on Day 30 normalized by total Cu in particle—was $Cu > Cu_2O >$ 10%Fe-CuO > 6%Fe-CuO > 2%Fe-CuO, 0%Fe-CuO, CuO-SA (Fig. A6). It is noteworthy that the dissolution rate of the particles may have decreased over time due to saturation, since the studies were carried out in a closed system. The initial dissolution rate is useful for predicting the behavior in open waters, and the trends observed here should be valid for natural systems.

Colloidal stability studies showed that the Fe-doped CuO NPs became less stable with increasing Fe-doping (Fig. 4) due to the decreasing magnitude of ζ potential (Fig. 3). Additionally, dissolution increased with Fe-doping, which led to higher concentrations of aqueous $Cu^{2+}$ in 6%Fe-CuO and 10%Fe-CuO, and that could have caused some subtle effects on the electrostatic double layers around these particles—further decreasing their colloidal stability in water. As such we expected particulate Cu suspended in water to decrease with increasing Fe-doping. However, we found more suspended Cu in these highly doped CuO NPs compared to 0%Fe-CuO and 2%Fe-CuO (Fig. 5c). We hypothesized that the observed slower settling of 6%Fe-CuO and 10%Fe-CuO (than expected) is probably due to decreases in the particle density upon doping with Fe, since the density of $CuFe_2O_4$ can be 13–38% less than that of CuO (Ali et al., 2011). The faster settling of 10%Fe-CuO than 6%Fe-CuO at the early stage of the experiment suggests that other factors not considered here also play a role in the settling of Fe-doped CuO, and requires further investigation.

Based on the abundance of the different size fractions analyzed, the particles detected in water suspensions were mostly (≥50%) larger than 200 nm in diameter (Fig. 5d). However, as shown in Fig. 6, these large-sized particles are mainly made up of aggregated nanosized particles held together by van der Waals attraction. TEM analyses showed similar morphology of 0%Fe-CuO after initial exposure to water and after 30 d (Fig. 6a and c). However, several smaller-sized particles were observed in 10%Fe-CuO after 30 d (Fig. 6b and d), in addition to aggregated particles with diameter similar to the 0%Fe-CuO NPs. These smaller-sized particles suggest disintegration of Fe-CuO NPs, or the recrystallization of dissolved ions. Further studies are needed to confirm either of these hypotheses, but the atomic data obtained via EDS analyses (Fig. A7 and A8) suggest that Cu formed complexes with other anions in water.

### 3.5. Toxicity to marine phytoplankton

The impact of 0%Fe-CuO, 10%Fe-CuO and CuO-SA (for comparison) on the growth of *I. galbana* was monitored for 5 d, when the cells are in exponential growth phase. In general, all three particle types had negligible effects on the growth of *I. galbana* (Fig. 7a–c and Fig. A9). Effects of NPs on algae was estimated as growth inhibition (I), which showed that the growth of *I. galbana* was either enhanced or inhibited by less than an average of 4% at all the concentrations considered (Fig. 7d). Statistically, while the NP type (0%Fe-CuO, 10%Fe-CuO or CuO-SA) had a significant effect on 5-day algal growth rate ($p < .0001$), NP concentration had no significant effect ($p = .16$). More so, the interaction of NP type and NP concentration had no significantly influence on the growth rate of algae in this study ($p = .70$), which explains our observation of no serious effects at all the conditions studied.

The toxicity of CuO NPs has often been attributed to dissolved Cu ions leaching out of the particles, intracellular dissolution of the NPs upon uptake by cells or organisms, and oxidative stress (Gomes et al., 2011; Gunawan et al., 2011; Ingle et al., 2014; Torres-Duarte et al., 2016; Wang et al., 2011b; Zhao et al., 2016a). Uptake of CuO NPs via endocytosis by microalgae is more common in freshwater systems since rapid aggregation and subsequent sedimentation of the NPs occur in marine systems (Perreault et al., 2012; Wang et al., 2011b; Zhao et al., 2016a). We reported in a previous study that CuO NPs (both commercial and in-house synthesized) aggregated to micrometer-scale within minutes of releasing them into a natural seawater, consequently leading to more than 60% settling out of aqueous phase within a few hours (Torres-Duarte et al., 2016). We therefore expected most of the toxicity to the organisms used in

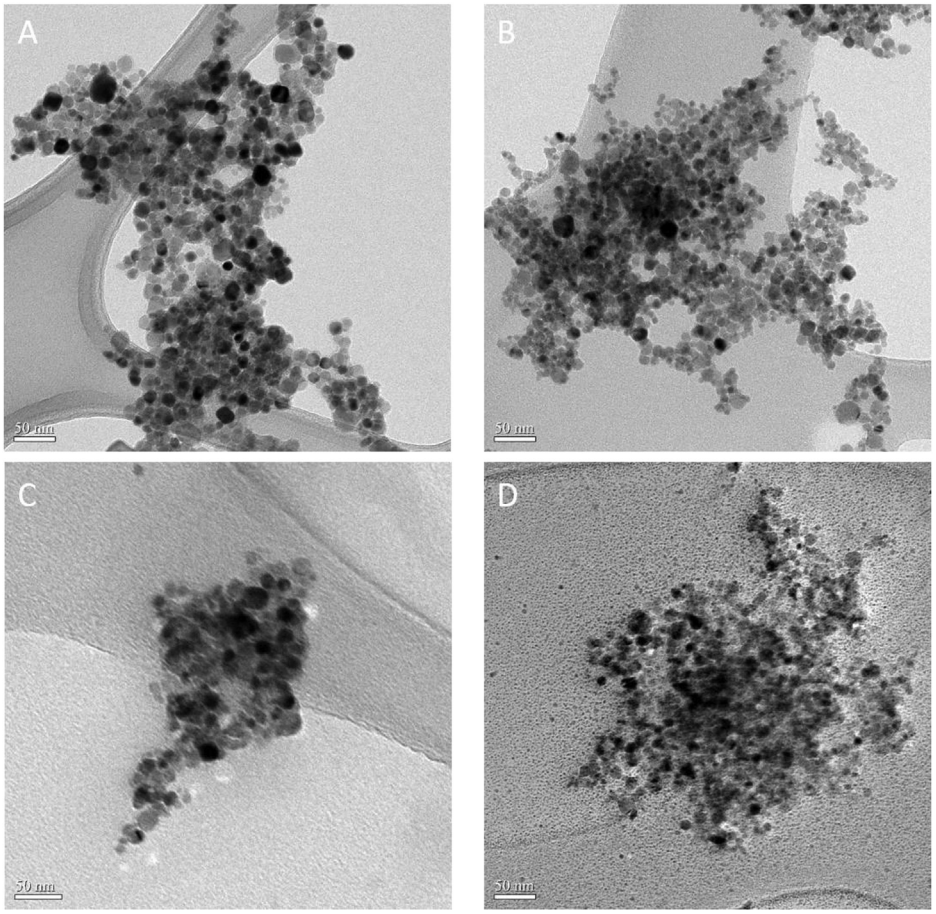


**Fig. 6.** Transmission electron micrographs of pure and Fe-doped CuO nanomaterials after their exposure to freshwater. (A) and (B) are 0%Fe-CuO and 10%Fe-CuO, respectively, after exposure to water for 2 h (C) and (D) are 0%Fe-CuO and 10%Fe-CuO, respectively, after exposure to water for 30 d. The scale bars represent 50 nm. The corresponding energy-dispersive X-ray spectroscopy (EDS) data are shown in Fig. A7 and A8.

this study to emanate from dissolved Cu, with 10%Fe-CuO having more effects because of its higher dissolution rate.

ICP-MS analyses of aliquots of culture media carried out during toxicity testing (on Days 1, 3, and 5) showed very low dissolved Cu concentrations, although more dissolution occurred in the Fe-doped CuO (similar to our finding in the dissolution studies). As shown in Fig. A10a, dissolved Cu concentration was below 0.5 mg/L over 5 d at all the concentrations of the NPs tested (with dissolution rate decreasing with increased particle concentration, Fig. A10b). Dissolved Cu detected in the culture media are predicted to be mostly complexed (Fig. A10c), based on modeling using Visual MINTEQ 3.1; and complexed Cu tend to be less toxic and less catalytic than free Cu ions (Gunawan et al., 2011; Wang et al., 2013). Details on Visual MINTEQ modeling is provided in section A3 in the appendix. Cu speciation modeling predicts less than 0.4% dissolved Cu at 10 mg/L NP concentration, and a much smaller fraction as $Cu^{2+}$. ROS production by CuO NPs in aqueous media is primarily caused by Fenton-like chemistry through the $Cu^{+}/Cu^{2+}$ redox couple induced by the dissolved Cu fraction (Kuan et al., 2015; Wang et al., 2013). Similarly, Fe species produced by the Fe-doped CuO NPs (equations (7) and (8)) can also lead to ROS production. It is therefore not surprising that we did not observe elevation of intracellular ROS production in the algal cells when exposed to pure and Fe-doped CuO NPs (0–10 mg/L) compared to the control conditions (Fig. A11). Lack of toxicity to *I. galbana* by pure and Fe-doped CuO NPs at concentrations up to 10 mg/L is therefore adduced mainly to slow dissolution and complexation of dissolved Cu ions in natural waters. In acidic conditions or open waters, where more dissolution may occur, $Fe^{3+}$ produced by the Fe-doped CuO can catalyze additional production of hydroxyl radical in the presence of UV-light (equation (9)), which may increase the toxicity of the Fe-doped CuO NPs.

$$Fe^{3+} + H_2O \xrightarrow{h\nu} Fe^{2+} + OH^{\bullet} + H^{+} \quad (9)$$

## 4. Conclusions

Pure and Fe-doped CuO NPs were synthesized by incorporating up to 10 wt % Fe into the lattice of CuO using flame spray pyrolysis (FSP). In order to predict the environmental implications of the NPs, we studied their surface properties, colloidal stability, dissolution and transformation in natural waters, as well as their potential toxicity to phytoplankton. We found that:

- With increased doping, the surface charge of the Fe-CuO NPs in aqueous media approached the surface charge of the dopant ($CuFe_2O_4$), although pH, ionic strength, and SRNOM also played important roles in determining the surface charge
- The colloidal stability of the Fe-CuO NPs decreased with increased Fe-doping, with or without SRNOM. The presence of SRNOM improved the stability of the Fe-CuO NPs much more at pH 5.5 than at pH 8.2

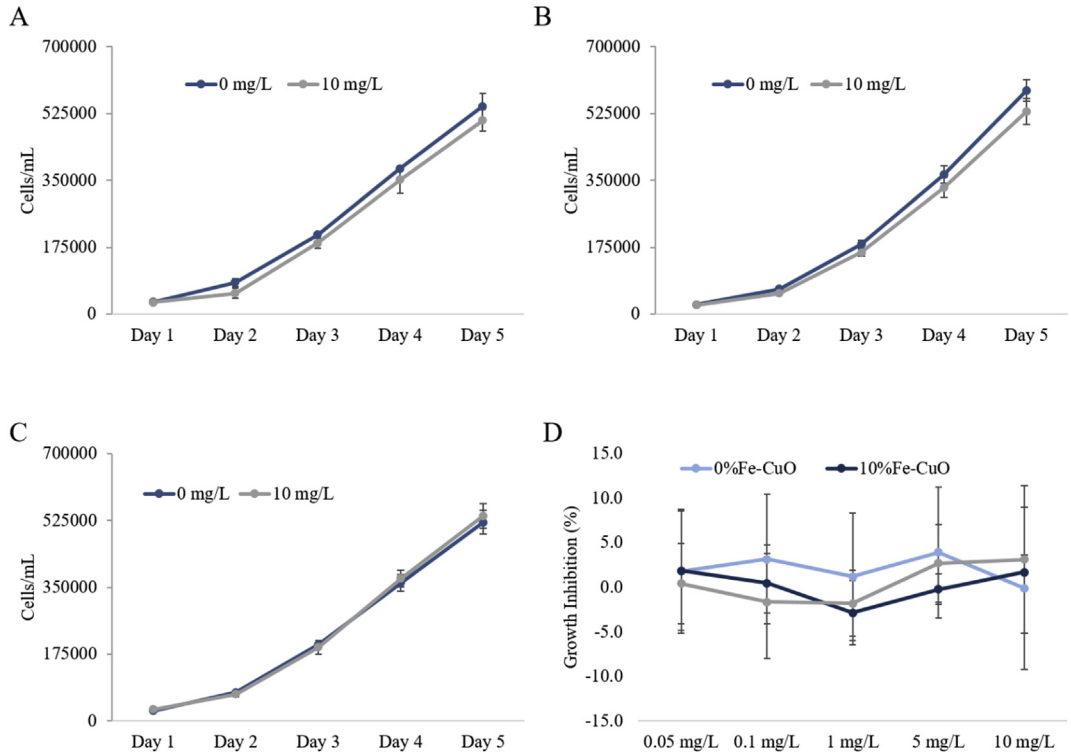


**Fig. 7.** Effects of 10 mg/L particle concentration of (A) 0%Fe-CuO, (B) 10%Fe-CuO, and (C) commercial CuO (CuO-SA) on the growth of *Isochrysis galbana* over 5 d. Data for particle concentrations between 0 and 10 mg/L is shown in the Appendix (Fig. A9). (D) Growth inhibition (%), of the three nanoparticles at exposure concentrations of 0, 0.05, 0.1, 1, and 10 mg/L relative to control conditions. Growth of *I. galbana* was either enhanced (I is negative) or inhibited (I is positive) by less than an average of 4% at all concentrations considered.

- Fe doping promoted dissolution of Fe-CuO NPs. Dissolved mass fraction was 0.52% and 0.81% after exposing 0%Fe-CuO and 10% Fe-CuO into freshwater for 24 h. Dissolution decreased with increased nanoparticle concentration
- There was minimal (less than 4% inhibition or enhancement) change in the rate of growth of *Isochrysis galbana* cells exposed to up to 10 mg/L of pure CuO NPs or 10%Fe-doped CuO NPs. This reflects the (1) relatively slow dissolution of Fe-doped CuO NPs in the growth media, and (2) complexation of most dissolved Cu present in the growth media, which reduces their toxicity.

## Acknowledgment

This material is based upon work supported by the National Science Foundation (NSF) and the Environmental Protection Agency under Cooperative Agreement Number DBI 0830117. Any opinions, findings, and conclusions or recommendations expressed in this material are those of the authors and do not necessarily reflect the views of NSF or EPA. We thank the MRL Central Facilities, which are supported by the MRSEC Program of the NSF under Award No. DMR 1121053, for the use of their instruments. The authors also thank Paige Rutten, Ekene A. Oranu, Robert J. Parker, and Anastasiia Minakova for lab assistance and data analyses. We also thank Caroline Vignardi and Prof. Hunter Lenihan for intracellular ROS analysis. S.P. and L.M. would like to thank Prof. A. Rosenauer for the TEM imaging of the dry powders. A.A.K. also appreciates Agilent Technologies for their Agilent Thought Leadership Award.

## Appendix A. Supplementary data

Supplementary data related to this article can be found at https://doi.org/10.1016/j.watres.2017.12.069.

## References

Adeleye, A.S., 2015. Influence of Phytoplankton and Extracellular Polymeric Substances on the Fate of Engineered Nanomaterials in Natural Aquatic Systems. University of California, Santa Barbara. PhD Thesis.
Adeleye, A.S., Conway, J.R., Garner, K., Huang, Y., Su, Y., Keller, A.A., 2016a. Engineered nanomaterials for water treatment and remediation: costs, benefits, and applicability. Chem. Eng. J. 286, 640–662.
Adeleye, A.S., Conway, J.R., Perez, T., Rutten, P., Keller, A.A., 2014. Influence of extracellular polymeric substances on the long-term fate, dissolution, and speciation of copper-based nanoparticles. Environ. Sci. Technol. 48 (21), 12561–12568.
Adeleye, A.S., Keller, A.A., 2014. Long-term colloidal stability and metal leaching of single wall carbon nanotubes: effect of temperature and extracellular polymeric substances. Water Res. 49 (0), 236–250.
Adeleye, A.S., Oranu, E.A., Tao, M., Keller, A.A., 2016b. Release and detection of nanosized copper from a commercial antifouling paint. Water Res. 102, 374–382.
Ali, K., Iqbal, A., Ahmad, M.R., Jamil, Y., Khan, S.A., Amin, N., Iqbal, M.A., Jafri, M.Z.M., 2011. Structural characterization of CuFe2O4 nanocomposites and synthesis by an economical method. Sci. Int. 23, 21–25.
Bennett, S.W., Adeleye, A., Ji, Z., Keller, A.A., 2013. Stability, metal leaching, photoactivity and toxicity in freshwater systems of commercial single wall carbon nanotubes. Water Res. 47 (12), 4074–4085.
Chen, W., Zhang, J.Z., Joly, A.G., 2004. Optical properties and potential applications of doped semiconductor nanoparticles. J. Nanosci. Nanotechnol. 4 (8), 919–947.
Conway, J.R., Adeleye, A.S., Gardea-Torresdey, J., Keller, A.A., 2015. Aggregation, dissolution, and transformation of copper nanoparticles in natural waters. Environ. Sci. Technol. 49 (5), 2749–2756.
De Volder, M.F.L., Tawfick, S.H., Baughman, R.H., Hart, A.J., 2013. Carbon nanotubes: present and future commercial applications. Science 339 (6119), 535–539.
Ding, Y., Zhu, L., Wang, N., Tang, H., 2013. Sulfate radicals induced degradation of tetrabromobisphenol A with nanoscaled magnetic CuFe2O4 as a heterogeneous catalyst of peroxymonosulfate. Appl. Catal. B Environ. 129 (Suppl. C), 153–162.
Dreyer, J.A., Pokhrel, S., Birkenstock, J., Hevia, M.G., Schowalter, M., Rosenauer, A., Urakawa, A., Teoh, W.Y., Mädler, L., 2016. Decrease of the required dopant concentration for δ-Bi 2 O 3 crystal stabilization through thermal quenching during single-step flame spray pyrolysis. Cryst. Eng. Comm 18 (12), 2046–2056.

EPA, U., 2002. Method 1003.0 in Short-term Methods for Estimating the Chronic Toxicity of Effluents and Receiving Waters to Freshwater Organisms. US EPA, Washington DC.
Everett, D., 1988. Basic Principles of Colloid Science.
Fairbairn, E.A., Keller, A.A., Mädler, L., Zhou, D., Pokhrel, S., Cherr, G.N., 2011. Metal oxide nanomaterials in seawater: linking physicochemical characteristics with biological response in sea urchin development. J. Hazard Mater. 192 (3), 1565–1571.
George, S., Pokhrel, S., Xia, T., Gilbert, B., Ji, Z., Schowalter, M., Rosenauer, A., Damoiseaux, R., Bradley, K.A., Mädler, L., Nel, A.E., 2010. Use of a rapid cytotoxicity screening approach to engineer a safer zinc oxide nanoparticle through iron doping. Action Natl. 4 (1), 15–29.
Gomes, T., Pinheiro, J.P., Cancio, I., Pereira, C.G., Cardoso, C., Bebianno, M.J., 2011. Effects of copper nanoparticles exposure in the mussel Mytilus galloprovincialis. Environ. Sci. Technol. 45 (21), 9356–9362.
Gunawan, C., Teoh, W.Y., Marquis, C.P., Amal, R., 2011. Cytotoxic origin of copper(II) oxide nanoparticles: comparative studies with micron-sized particles, leachate, and metal salts. Action Natl. 5 (9), 7214–7225.
Hong, Y., Hu, H.-Y., Xie, X., Sakoda, A., Sagehashi, M., Li, F.-M., 2009. Gramine-induced growth inhibition, oxidative damage and antioxidant responses in freshwater cyanobacterium Microcystis aeruginosa. Aquat. Toxicol. 91 (3), 262–269.
Ingle, A.P., Duran, N., Rai, M., 2014. Bioactivity, mechanism of action, and cytotoxicity of copper-based nanoparticles: a review. Appl. Microbiol. Biotechnol. 98 (3), 1001–1009.
Ivask, A., Titma, T., Visnapuu, M., Vija, H., Kakinen, A., Sihtmae, M., Pokhrel, S., Madler, L., Heinlaan, M., Kisand, V., 2015. Toxicity of 11 metal oxide nanoparticles to three mammalian cell types in vitro. Curr. Top. Med. Chem. 15 (18), 1914–1929.
Keller, A.A., Adeleye, A.S., Conway, J.R., Garner, K.L., Zhao, L., Cherr, G.N., Hong, J., Gardea-Torresdey, J.L., Godwin, H.A., Hanna, S., Ji, Z., Kaweeteerawat, C., Lin, S., Lenihan, H.S., Miller, R.J., Nel, A.E., Peralta-Videa, J.R., Walker, S.L., Taylor, A.A., Torres-Duarte, C., Zink, J.I., Zuverza-Mena, N., 2017. Comparative environmental fate and toxicity of copper nanomaterials. NanoImpact 7 (Suppl. C), 28–40.
Keller, A.A., McFerran, S., Lazareva, A., Suh, S., 2013. Global life cycle releases of engineered nanomaterials. J. Nanoparticle Res. 15 (6), 1–17.
Kemmler, J.A., Pokhrel, S., Mädler, L., Weimar, U., Barsan, N., 2013. Flame spray pyrolysis for sensing at the nanoscale. Nanotechnology 24 (44), 442001.
Kuan, C.-C., Chang, S.-Y., Schroeder, S.L.M., 2015. Fenton-like oxidation of 4-chlorophenol: homogeneous or heterogeneous? Ind. Eng. Chem. Res. 54 (33), 8122–8129.
Li, Y., Yang, L., Liu, X., Li, N., Zhang, L., Li, Q., Yang, Y., Duan, Y., Zhang, F., 2015. Highly enhanced selectivity for the separation of rhenium and molybdenum using amino-functionalized magnetic Cu-ferrites. J. Mater. Sci. 50 (18), 5960–5969.
Midander, K., Cronholm, P., Karlsson, H.L., Elihn, K., Möller, L., Leygraf, C., Wallinder, I.O., 2009. Surface characteristics, copper release, and toxicity of nano- and micrometer-sized copper and copper(II) oxide particles: a cross-disciplinary study. Small 5 (3), 389–399.
Naatz, H., Lin, S., Li, R., Jiang, W., Ji, Z., Chang, C.H., Köser, J., Thöming, J., Xia, T., Nel, A.E., Mädler, L., Pokhrel, S., 2017. Safe-by-Design CuO nanoparticles via Fe-Doping, Cu–O Bond length variation, and biological assessment in cells and zebrafish embryos. ACS Nano 11 (1), 501–515.
Perreault, F., Oukarroum, A., Melegari, S.P., Matias, W.G., Popovic, R., 2012. Polymer coating of copper oxide nanoparticles increases nanoparticles uptake and toxicity in the green alga Chlamydomonas reinhardtii. Chemosphere 87 (11), 1388–1394.
Pokhrel, S., Birkenstock, J., Dianat, A., Zimmermann, J., Schowalter, M., Rosenauer, A., Ciacchi, L.C., Mädler, L., 2015. In situ high temperature X-ray diffraction, transmission electron microscopy and theoretical modeling for the formation of WO 3 crystallites. Cryst. Eng. Comm 17 (36), 6985–6998.
Pokhrel, S., Birkenstock, J., Schowalter, M., Rosenauer, A., Mädler, L., 2010. Growth of ultrafine single crystalline WO3 nanoparticles using flame spray pyrolysis. Cryst. Growth Des. 10 (2), 632–639.
Thakar, R., Chen, Y.C., Snee, P.T., 2007. Efficient emission from core/(doped) shell nanoparticles: applications for chemical sensing. Nano Lett. 7 (11), 3429–3432.
Torres-Duarte, C., Adeleye, A.S., Pokhrel, S., Mädler, L., Keller, A.A., Cherr, G.N., 2016. Developmental effects of two different copper oxide nanomaterials in sea urchin (Lytechinus pictus) embryos. Nanotoxicology 10 (6), 671–679.
Wagner, H.D., 2007. Nanocomposites: paving the way to stronger materials. Nat. Nanotechnol. 2 (12), 742–744.
Wang, G.F., Peng, Q., Li, Y.D., 2011a. Lanthanide-doped nanocrystals: synthesis, optical-magnetic properties, and applications. Accounts Chem. Res. 44 (5), 322–332.
Wang, Z., Li, J., Zhao, J., Xing, B., 2011b. Toxicity and internalization of CuO nanoparticles to prokaryotic alga microcystis aeruginosa as affected by dissolved organic matter. Environ. Sci. Technol. 45 (14), 6032–6040.
Wang, Z., von dem Bussche, A., Kabadi, P.K., Kane, A.B., Hurt, R.H., 2013. Biological and environmental transformations of copper-based nanomaterials. ACS Nano. 7 (10), 8715–8727.
Xia, T., Zhao, Y., Sager, T., George, S., Pokhrel, S., Li, N., Schoenfeld, D., Meng, H., Lin, S., Wang, X., Wang, M., Ji, Z., Zink, J.I., Mädler, L., Castranova, V., Lin, S., Nel, A.E., 2011. Decreased dissolution of ZnO by iron doping yields nanoparticles with reduced toxicity in the rodent lung and zebrafish embryos. ACS Nano 5 (2), 1223–1235.
Yin, S., Yuan, S., Tian, Z., Liu, L., Wang, C., Zheng, X., Duan, H., Huo, S., 2010. Effect of particle size on the exchange bias of Fe-doped CuO nanoparticles. J. Appl. Phys. 107 (4), 043909.
Zhao, J., Cao, X., Liu, X., Wang, Z., Zhang, C., White, J.C., Xing, B., 2016a. Interactions of CuO nanoparticles with the algae Chlorella pyrenoidosa: adhesion, uptake, and toxicity. Nanotoxicology 10 (9), 1297–1305.
Zhao, L., Ortiz, C., Adeleye, A.S., Hu, Q., Zhou, H., Huang, Y., Keller, A.A., 2016b. Metabolomics to detect response of lettuce (Lactuca sativa) to Cu (OH) 2 nanopesticides: oxidative stress response and detoxification mechanisms. Environ. Sci. Technol. 50 (17), 9697–9707.